Chinese Chemical Letters 33 (2022) 1395–1402

Contents lists available at ScienceDirect

Chinese Chemical Letters

journal homepage: www.elsevier.com/locate/cclet

Synthesis of Co_4S_3/Co_9S_8 nanosheets and comparison study toward the OER properties induced by different metal ion doping

Fenghua Chen[a,*], Zhaoqian Zhang[a], Weiwei Liang[a], Xiaoyun Qin[a], Zhen Zhang[b,*], Liying Jiang[c]

[a] College of Materials and Chemical Engineering, Zhengzhou University of Light Industry, Zhengzhou 450002, China
[b] Tianjin Key Laboratory of Molecular Optoelectronic Department of Chemistry, School of Science, Tianjin University, Tianjin 300072, China
[c] School of Electrical and Information Engineering, Zhengzhou University of Light Industry, Zhengzhou 450002, China

ARTICLE INFO

Article history:
Received 19 June 2021
Revised 16 July 2021
Accepted 5 August 2021
Available online 11 August 2021

Keywords:
Chalcogenides
Chemical synthesis
Catalytic properties
Doping
Nanosheets
OER

ABSTRACT

Regulation of chemical composition and nanostructure, such as the introduction of dopant into two-dimensional nanomaterials, is a general and valid strategy for the efficient electrocatalyst design. In this work, Co_4S_3/Co_9S_8 nanosheets, with an ultrathin layer structure, were successfully synthesized *via* an efficient solvothermal process combined with ultrasonic exfoliation. Different metal ions ($M = Fe^{3+}$, Cr^{3+}, Mn^{2+} and Ni^{2+}) were then doped by a simple cation exchange method and the effects of different dopants on the OER activities of Co_4S_3/Co_9S_8 NS were further investigated in alkaline media. The corresponding results implied that M-doped Co_4S_3/Co_9S_8 NS ($M = Fe^{3+}$, Cr^{3+}, Mn^{2+} and Ni^{2+}) exhibited different electrocatalytic properties. Evidenced by XPS spectra, the different OER activities were mainly aroused by the redistribution of charge at the interface due to an electronic interaction between the doped metal ions and Co_4S_3/Co_9S_8 NS.

Due to its simplicity, cost-effectiveness and cleanness, electrochemical approach has attracted considerable interest in water splitting into oxygen and hydrogen, which is of great importance to sustainable renewable energy resources [1-3]. However, owing to the relatively slow kinetics of oxygen evolution reaction (OER) at the anode and the low conversion efficiency of water to fuel, efficient electrocatalyst is thus desperate needed to reduce the activation energy barrier [4,5].

Over the past several decades, due to the wide stoichiometric composition and intrinsic activities, various abundant and productive compounds containing 3d transition metals, especially cobalt chalcogenides, have been developed as promising alternatives for noble-metal oxygen evolution reaction (OER) catalyst [6-8], the shortcomings of which are the elemental scarcity and worse stability. Many literatures have reported that the activities of cobalt sulfide catalysts partly depend on their morphology and the microchemical environment of cobalt active sites [9-11]. In comparsion with various different morphologies of cobaltchalcogenides-based electrode materials, two-dimensional nanosheet materials usually show promising electrocatalytic performance due to their advantages of large specific surface area and fast charge transfer capacity [12,13], which has attracted extensive attention. The further tuning of chemical composition and nanostructures are expected to be a general and valid strategy for the improvement of OER reactivity [14]. To tailor the chemical composition of electrocatalysts, the introducing of doping ions into the crystal lattice of materials has become an effective route to manipulate the electrical properties [15,16]. It has been confirmed in the literatures that the $Co(OH)_2$ [17], $Ni(OH)_2$ [18,19], TiO_2 [20-22] and MnO_2 [23] composites electrode all exhibit greatly enhanced OER activity after the doping by Fe, Cu, Co and V, respectively. However, there are few reports about the effects of different dopants on the electrocatalytic performance of one catalyst. For cobalt sulfide-based electrocatalyst, only Fe ions and Ni ions have been reported to influence active-phase structure and significantly improve the OER catalysis activity [24,25]. To the best of our best knowledge, there are still few reports about the synthesis Co_4S_3/Co_9S_8 nanosheets and the effects of the different doped metal ions on its OER electrocatalytic properties for oxygen evolution reaction.

Here, we present an efficient solvothermal process combined with ultrasonic exfoliation for the synthesis of Co_4S_3/Co_9S_8 nanosheets (Co_4S_3/Co_9S_8 NS). With the followed simple cation exchange method, we further prepared M-doped Co_4S_3/Co_9S_8 NS ($M = Fe^{3+}$, Cr^{3+}, Mn^{2+} and Ni^{2+}) at room temperature and compared their OER activities in alkaline media. The corresponding re-

* Corresponding authors.
E-mail addresses: phenix@zzuli.edu.cn (F. Chen), zhzhen@tju.edu.cn (Z. Zhang).

https://doi.org/10.1016/j.cclet.2021.08.019
1001-8417/

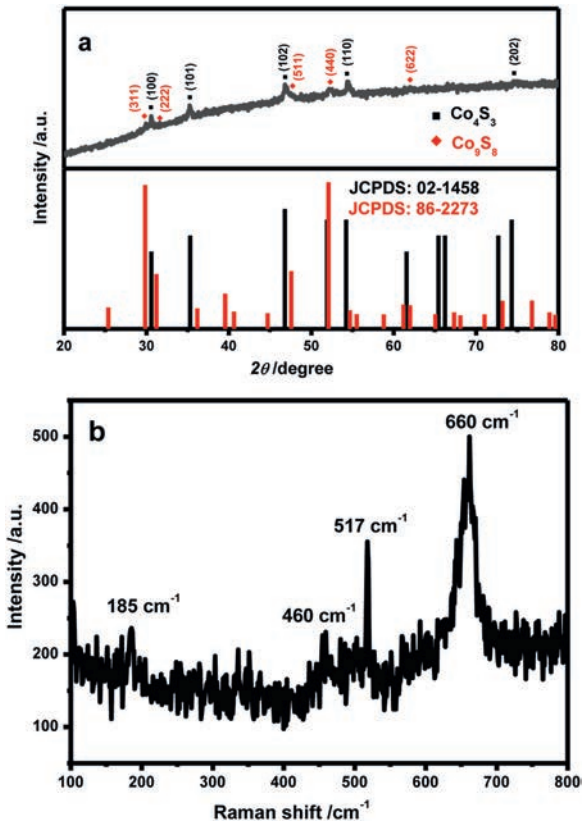

Fig. 1. (a) XRD patterns and (b) Raman spectrum of Co_4S_3/Co_9S_8 nanosheets.

sults implied that M-doped Co_4S_3/Co_9S_8 NS (M = Fe^{3+}, Cr^{3+}, Mn^{2+} and Ni^{2+}) exhibited different electrocatalytic properties. Towards such different influences of the different metal ions doping on the electrocatalytic properties for oxygen evolution reaction, XPS analysis were carried out to investigate the possible reasons.

The details of the preparation process,structure and morphology characterization and the OER electrocatalytic performance tests of Co_4S_3/Co_9S_8 NS and M-doped Co_4S_3/Co_9S_8 NS (M = Fe^{3+}, Cr^{3+}, Mn^{2+} and Ni^{2+}) can be seen in Supporting information.

According to the so-called "solvent coordination molecular template strategy" [23,26-28], that was, the DETA was embedded between adjacent cobalt sulfide layers through the Co-N coordination, and then Co_4S_3/Co_9S_8 nanosheets with two-dimensional lamellar structure were obtained by ultrasound exfoliation treatment from an intermediate Co_4S_3/Co_9S_8-DETA hybrid precursor. The crystallinity and composition of the cobaltous sulfide were determined by the powder XRD patterns. From Fig. 1a, the characteristic peaks indexed to (100), (101), (102), (110) and (202) crystal planes of Co_4S_3 (JCPDS No. 02-1458) can be seen at 30.6°, 35.3°, 46.8°, 54.4° and 74.6°, respectively. Consulting the JCPDS No. 86-2273, the peaks located at the position of 29.8°, 31.5°, 47.7°, 52.2° and 61.9° can well correspond to the (311), (222), (511), (440) and (622) planes of the co-existence Co_9S_8, respectively. There were no extra diffraction peaks in the XRD pattern other than Co_4S_3 and Co_9S_8, indicating highly purified products of Co_4S_3/Co_9S_8 NS. Raman spectroscopy of Co_4S_3/Co_9S_8 NS was further performed to confirm the chemical physical environment. The Raman spectrum of the typical Co_4S_3/Co_9S_8 NS was shown in Fig. 1b. Four well-resolved Raman peaks were seen at 185 cm^{-1}, 460 cm^{-1}, 517 cm^{-1} and 660 cm^{-1}, which were perfectly indexed to the F_{2g}, E_g, F_{2g} and A_{1g} modes of cobalt sulfide, respectively [29-31].

Figs. 2a and b showed the TEM and SEM images of the synthesized Co_4S_3/Co_9S_8 samples. The remarkable morphology of two-dimensional nanosheets can be clearly distinguished. The distribution of cobalt and sulfur elements can be obtained by elemental mapping images of the SEM image of Co_4S_3/Co_9S_8 NS in Fig. S1 (Supporting information). The crystalline structure of Co_4S_3/Co_9S_8 composite was further confirmed from the electron diffraction patterns of selected area (SAED). As shown in Fig. 2c, a clear crystalline spot ring, which belonged to the polycrystalline structure with the indexed planes of Co_4S_3 (100), (101), (102), (110) and (202) and Co_9S_8 (622), matched well with the results of XRD, further confirming the formation of Co_4S_3/ Co_9S_8 composites. The results of AFM in Fig. 2d demonstrated that the height of Co_4S_3/Co_9S_8 nanosheets was 1∼2 nm, indicating an ultrathin layer structure.

To identify the bonding configuration, Fig. 3 illustrated the high-resolution Co 2p and S 2p XPS spectra of Co_4S_3/Co_9S_8 NS, which had been fitted by Gaussian method. Two spin-orbit doublets and two shakeup satellites (denoted as "Sat.") could be fitted for the core level of Co 2p. The fitting peaks of Co 2p located at 778.8 eV and 793.6 eV and the other fitting peaks of Co 2p at 780.4 eV and 796.5 eV were attributed to Co^{2+} and Co^{3+}, respectively, the two categories of cobalt oxidation states existed in Co_4S_3/Co_9S_8 NS [32,33]. In the S 2p spectrum (Fig. 3b), the asymmetric peaks at 161.5 eV and 162.8 eV were indexed to the S $2p_{3/2}$ and S $2p_{1/2}$ peaks of cobalt sulfide nanosheets, while binding energy of 167.6 eV can be assigned to the satellite peak of sulfur. Hence, based on the above XPS analysis, the successful formation of Co_4S_3/Co_9S_8 NS can be further verified.

XPS characterization of the Co_4S_3/Co_9S_8 NS catalyst after OER reaction was also carried out here to ascertain whether there was a possibility of component and structural evolution during the OER process of the prepared Co_4S_3/Co_9S_8 NS catalyst. In the Co 2p and S 2p spectra of Co_4S_3/Co_9S_8 NS after OER under alkaline conditions (Figs. 3a and b), it was noteworthy that the Co $2p_{3/2}$ and Co $2p_{1/2}$ peaks exhibited 0.3 eV and 0.4 eV negative shifts, respectively, while that the S $2p_{3/2}$ and S $2p_{1/2}$ peaks exhibited 0.4 eV and 0.3 eV positive shifts, respectively. This experimental phenomenon showed that there existed electron transfer between cobalt and sulfur, and both the electron states on the surface of cobalt and sulfur atoms had been regulated. The negative shifts of Co 2p after the OER reaction compared with the pristine Co_4S_3/Co_9S_8 NS indicated a lower oxidation state of Co species. Besides, the Co $2p_{3/2}$ peak located at 780.0 eV evidenced the still existence of Co-S bond after the OER reaction [34]. Thus, combined with the fact that the doublets appearing at 781.5 eV and 796.1 eV can be attributed to Co^{3+} $2p_{3/2}$ and Co^{3+} $2p_{1/2}$ of Co_9S_8, we can infer that the sample after OER reaction was still cobalt-sulfur compound with the higher content of cobalt species of low oxidation state. However, owing to the strong affinity to O of Co^{2+}, cobalt hydroxide may also be formed due to absorbed hydroxide species under alkaline conditions during the OER process. To verify this, XRD patterns of the catalysts after OER reaction were performed and the results were illustrated in Fig. 4. It was obvious that after the OER reaction, the component of the catalyst was still Co_4S_3/Co_9S_8 and no cobalt hydroxide products were formed. What was slightly different was that the structure of Co_4S_3 has been partially transformed. Therefore, according to the analysis of the above results, the Co_4S_3/ Co_9S_8 catalyst as-prepared was "true catalyst", which was responsible for the catalytic activity in OER.

As mentioned above, ion doping can regulate the OER properties of electrocatalyst effectively [15,16]. The literatures have showed that cation exchange reaction is an extremely versatile and simple tool for the accessing novel nanomaterials, and also a powerful postsynthetic modification strategy that changes the composition of one nanomaterial while maintaining its morphology and crystal structure [35,36]. Compared with bulk extended solids, due to the relatively small number of atomic layers and

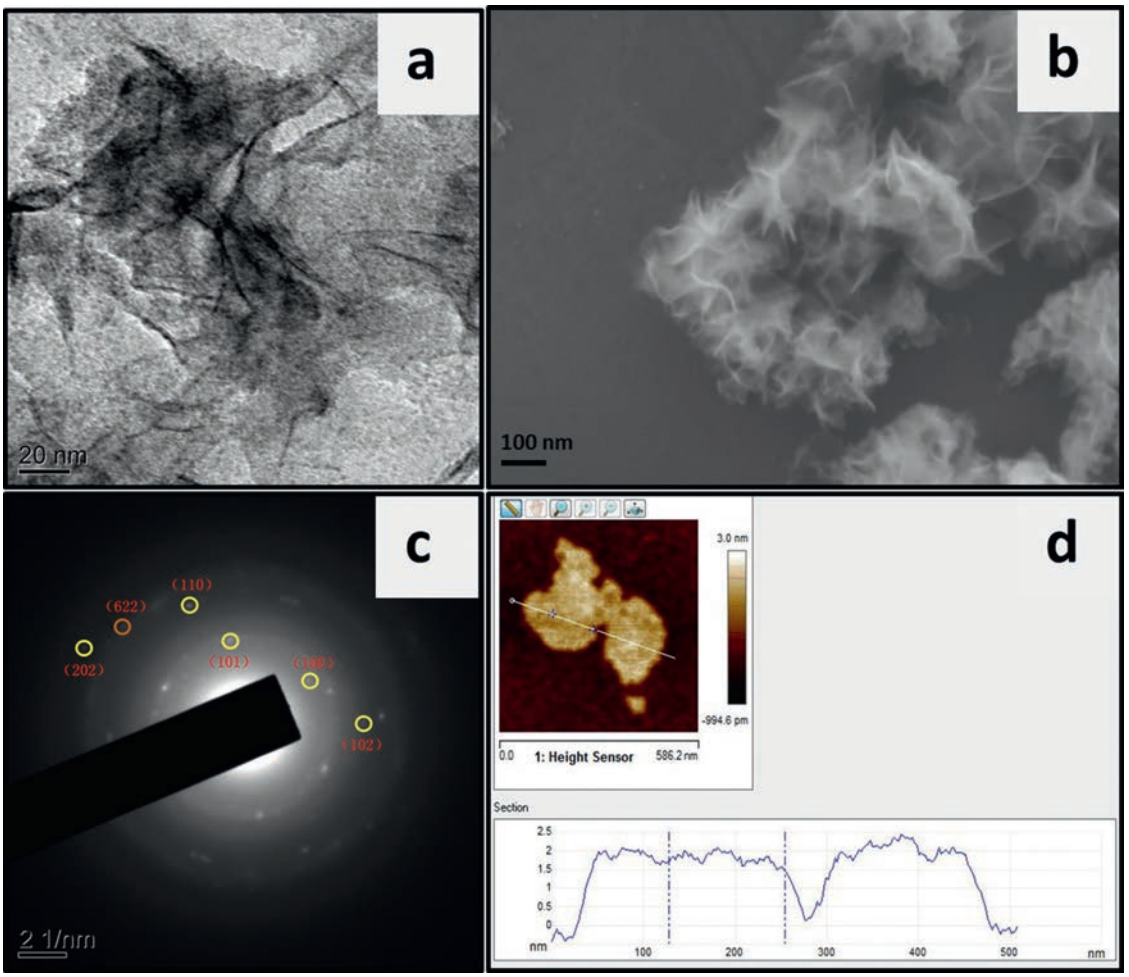

Fig. 2. (a) TEM image, (b) SEM image, (c) SAED patterns and (d) AFM image of the prepared Co_4S_3/Co_9S_8 nanosheets.

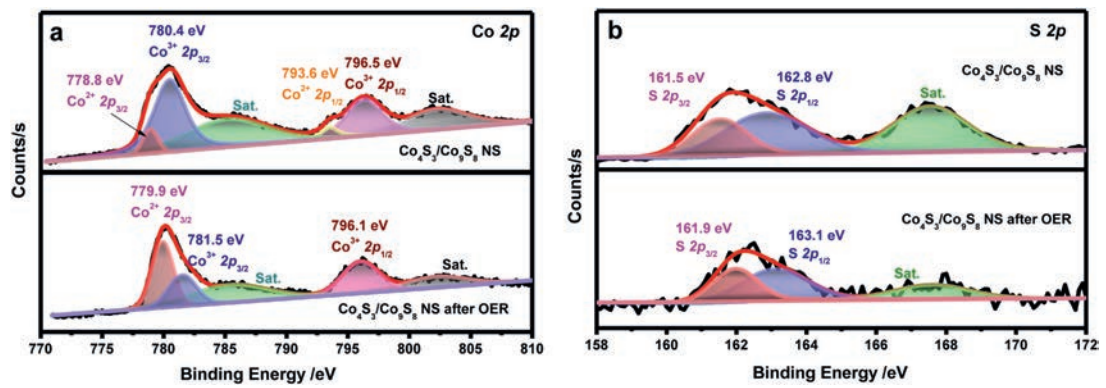

Fig. 3. Surface chemical states of Co_4S_3/ Co_9S_8 NS before and after OER: (a) High resolution XPS spectra of Co 2p; (b) High resolution XPS spectra of S 2p.

the highly reactive cobalt atoms for the ultrathin two-dimensional Co_4S_3/Co_9S_8 nanomaterials, cation exchange reaction can occur completely and reversibly in ionic nanosheets at room temperature with unusually fast reaction rates [37,38]. So herein, we selected the cation exchange method to prepare the M-doped Co_4S_3/Co_9S_8 NS (M = Fe^{3+}, Cr^{3+}, Mn^{2+} and Ni^{2+}), in which the cobalt cations ligated within a nanocrystal host lattice were substituted with Fe^{3+}, Cr^{3+}, Mn^{2+} and Ni^{2+} cations in solution, respectively.

Based on the LSV data of the four Fe-doped catalyst samples with different feeding molar rations of Fe/Co during the synthesis process of Fe-doped Co_4S_3/Co_9S_8 NS shown in Fig. S2 (Supporting information), we found that 30% Fe-doped Co_4S_3/Co_9S_8 NS exhibited the highest catalytic activity and power to derive the OER among the four Fe-doped catalysts. Therefore, herein, the OER properties of different metal ions (M = Fe^{3+}, Cr^{3+}, Mn^{2+} and Ni^{2+}) doped Co_4S_3/Co_9S_8 NS prepared with the same feeding mole rations of M/Co (3:10) were compared. As illustrated in Fig. S3 (Supporting information), Fe, Cr, Mn and Ni signals can be clearly detected in the survey XPS spectra of four M-doped Co_4S_3/Co_9S_8 NS (M = Fe^{3+}, Cr^{3+}, Mn^{2+} and Ni^{2+}), indicating the successful doping of the metal ions into Co_4S_3/Co_9S_8 NS. The distribution of cobalt, sulfur and the respective doped metallic elements can also be dis-

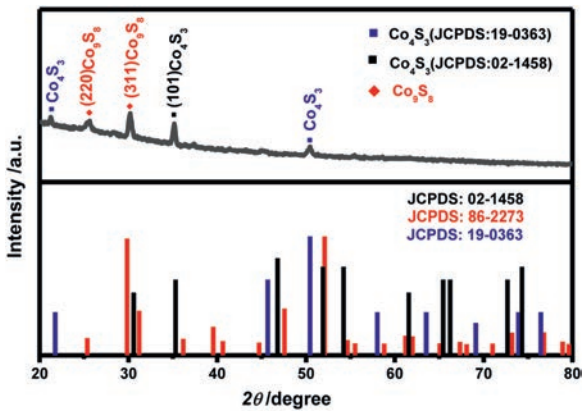

Fig. 4. XRD patterns of the prepared Co_4S_3/ Co_9S_8 nanosheets after OER.

tinguished by elemental mapping images of their SEM images of M-doped Co_4S_3/Co_9S_8 NS (M = Fe^{3+}, Cr^{3+}, Mn^{2+} and Ni^{2+}) in Figs. S4-S7 (Supporting information), respectively.

The effects of different metal ions (M = Fe^{3+}, Cr^{3+}, Mn^{2+} and Ni^{2+}) doping on the electrochemical catalysis activity for OER of Co_4S_3/Co_9S_8 NS were investigated in alkaline media, which were first studied by LSV (Fig. 5a). From the detailed comparisons of the required overpotential to reach a current density of 10 mA/cm^2 shown in Fig. 5b, we can see that the overpotentials at η_{10} for Co_4S_3/Co_9S_8 NS, Fe-doped Co_4S_3/Co_9S_8 NS, Cr-doped Co_4S_3/Co_9S_8 NS, Mn-doped Co_4S_3/Co_9S_8 NS, and Ni-doped Co_4S_3/Co_9S_8 NS were 398 mV, 354 mV, 386 mV, 396 mV and 414 mV, respectively. This result proved that the Co_4S_3/Co_9S_8NS exhibited enhanced electrocatalytic properties for OER after the Fe^{3+} doping, and the OER catalysis activities of Cr-doped Co_4S_3/Co_9S_8 NS and Mn-doped Co_4S_3/Co_9S_8 NS were just a little better than undoped Co_4S_3/Co_9S_8. However, what need to be pointed out was that the catalytic activity of Ni-doped Co_4S_3/Co_9S_8 NS on OER was obviously poor than other samples. This meant that the doping of Ni^{2+} ions weakened the catalytic activity for the OER. The catalytic kinetics of these samples was also confirmed by the Tafel plots, which were calculated from LSV curves in low overpotential regimes and were exhibited in Fig. 5c. It can be intuitively observed that Fe-doped Co_4S_3/Co_9S_8 NS had the smaller Tafel slope of 52.65 mV/dec than Co_4S_3/Co_9S_8 NS (59.22 mV/dec), Cr-doped Co_4S_3/Co_9S_8 NS (65.29 mV/dec), Mn-doped Co_4S_3/Co_9S_8 NS (62.70 mV/dec) and Ni-doped Co_4S_3/Co_9S_8 NS (85.63 mV/dec), implying that Fe-doped Co_4S_3/Co_9S_8 NS had the highest electrocatalytic activity and Ni-doped Co_4S_3/Co_9S_8 NS had the lowest catalytic activity and power to derive the OER among these five samples.The results for enhancing or weakening OER activities of the Co_4S_3/Co_9S_8 NS due to the metal ions doping could also be deduced from the charge transfer resistance, as indicated by the EIS results in Fig. 6a. It showed that Fe-doped Co_4S_3/Co_9S_8 NS had the smallest semicircular diameter, indicating a lower charge transfer resistance. Conversely, Ni-doped Co_4S_3/Co_9S_8 NS displayed a higher charge transfer resistance confirmed by the largest semicircular diameter.

We further compared the electrochemical surface area (ECSA), calculated based on their double-layer capacitance (C_{dl}), which was measured from the linear slope of capacitive current *vs.* scan rate in the non-Faraday potential region. As can be seen in Fig. 6b, the C_{dl} values of M-doped Co_4S_3/Co_9S_8 NS (M = Fe^{3+}, Cr^{3+}, Mn^{2+} and Ni^{2+}) were all significantly outperforming that of undoped Co_4S_3/Co_9S_8 NS. This phenomenon suggested that the introduced metal ions into Co_4S_3/Co_9S_8 NS, even though the metal ions were Ni^{2+},could provide more active sites for OER catalysis. However, the increase in electrochemical surface area was not the sole factor for activity enhancement [39]. So based on the above results including the η_{10}, Tafel slope and EIS values, we speculated that the OER catalysis abilities of Co_4S_3/Co_9S_8 NS and M-doped Co_4S_3/Co_9S_8 NS (M = Fe^{3+}, Cr^{3+}, Mn^{2+} and Ni^{2+}) were mainly due to their intrinsical charge transfer kinetics.

The stability of catalyst is another important parameter that determines the performance of a catalyst. The catalytic durability of these samples was evaluated by performing CA and CP measurements. The results of CA testing exhibited in Fig. 6c demonstrated that Fe-doped Co_4S_3/Co_9S_8 NS delivered the highest current densities at different overpotentials compared with Co_4S_3/Co_9S_8 NS, Cr-doped Co_4S_3/ Co_9S_8 NS, Mn-doped Co_4S_3/Co_9S_8 NS, and Ni-doped Co_4S_3/Co_9S_8 NS. Similarly, the lowest current densities were still produced by Ni-doped Co_4S_3/ Co_9S_8 NS, which was consistent with the above conclusions.The results of CP response recorded at a constant current density of 10 mA/cm^2 were shown in Fig. 6d. As can be seen, undoped Co_4S_3/Co_9S_8 NS suffered from gradually declining activity, with a remarkable overpotential increase of 67.2 mV in only 5 h. In comparison, Fe-doped Co_4S_3/Co_9S_8 NS, Cr-doped Co_4S_3/Co_9S_8 NS, and Mn-doped Co_4S_3/Co_9S_8 NS exhibited excellent catalytic stability. Although the overpotential of Ni-doped Co_4S_3/Co_9S_8 NS also had a tendency to increase, it was still more stable than Co_4S_3/Co_9S_8 NS.

To sum up, from the comparison of the OER activity tests of these five samples, Fe-doped Co_4S_3/Co_9S_8 NS showed the fairly betterOER catalytic activity than Co_4S_3/Co_9S_8 NS. The OER catalysis activities of Cr-doped Co_4S_3/Co_9S_8 NS and Mn-doped Co_4S_3/Co_9S_8 NS were just a little better than undoped Co_4S_3/Co_9S_8 NS. In contrast, Ni-doped Co_4S_3/Co_9S_8 NS displayed the lower OER catalysis activity than undoped Co_4S_3/Co_9S_8 NS. Therefore, although the catalytic performance of these five samples was not very good compared to the electrocatalytic data of benchmarked RuO_2 and IrO_2 electrocatalyst, the overpotentials at η_{10} of which is 287 mV [40] and 335 mV [41] in alkaline medium, respectively, the results in the present work can supply the trends in OER catalytic activity induced by different ion doping and provide a new way for structural engineering of transition-metal sulfide-based electrocatalysts.

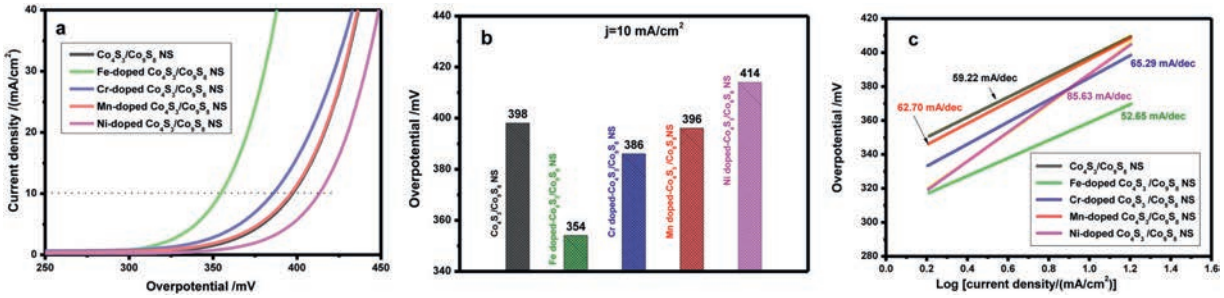

Fig. 5. OER catalytic performances of Co_4S_3/Co_9S_8NS, Fe-doped Co_4S_3/ Co_9S_8 NS, Cr-doped Co_4S_3/Co_9S_8 NS, Mn-doped Co_4S_3/Co_9S_8 NS and Ni-doped Co_4S_3/Co_9S_8NS: (a) LSV curves, (b) required over potentials at η_{10} and (c) Tafel plots derived from the polarization curves.

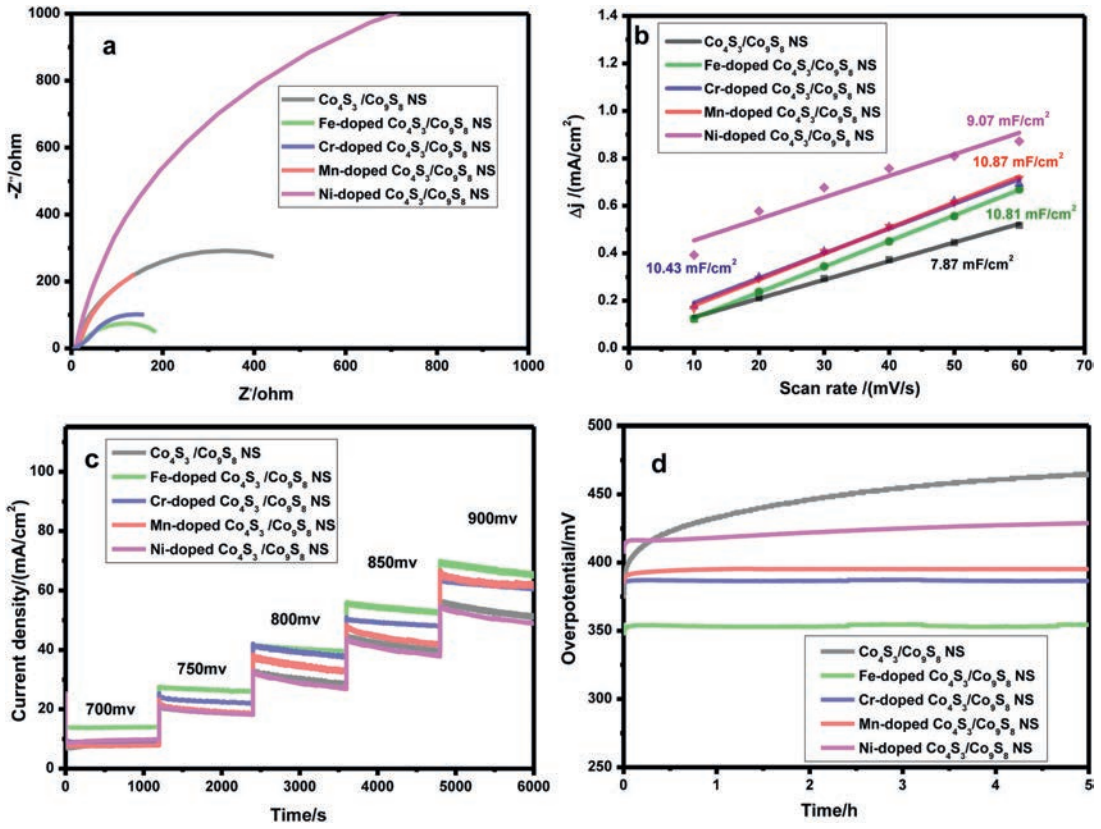

Fig. 6. OER catalytic performances of Co_4S_3/Co_9S_8NS, Fe-doped Co_4S_3/Co_9S_8 NS, Cr-doped Co_4S_3/Co_9S_8 NS, Mn-doped Co_4S_3/Co_9S_8 NS, and Ni-doped Co_4S_3/Co_9S_8 NS: (a) Nyquist plots; (b) electrochemical double-layer capacitance (C_{dl}); durability measurement by (c) a chronoamperometric test (CA) at stepwisely increased overpotential and (d) a chronopotentiometric test (CP) for 5 h.

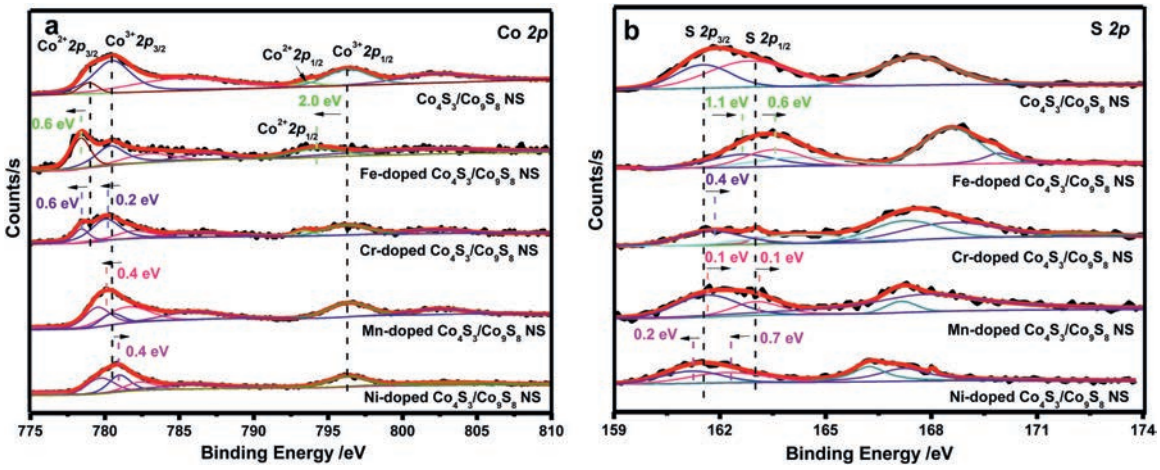

Fig. 7. Surface chemical states of Co_4S_3/Co_9S_8NS, Fe-doped Co_4S_3/Co_9S_8NS, Cr-doped Co_4S_3/Co_9S_8NS, Mn-doped Co_4S_3/Co_9S_8NS and Ni-doped Co_4S_3/Co_9S_8NS: (a) High resolution XPS spectra of Co 2p; (b) High resolution XPS spectra of S 2p.

XPS analysis was carried out to investigate the possible reasons towards the different influences of the different metal ions doping on the electrocatalytic properties for oxygen evolution reaction. Fig. 7 illustrated the high-resolution Co 2p and S 2p XPS spectra of these five Co_4S_3/Co_9S_8 NS based samples. Compared with undoped Co_4S_3/Co_9S_8 NS, the two typical peaks assigned to the chemical states of Co^{2+} $2p_{3/2}$ and Co^{2+} $2p_{1/2}$ in Fe-doped Co_4S_3/Co_9S_8 NS exhibited 0.6 eV and 2.0 eV negative shifts, respectively (Fig. 7a). Besides, the ratio of cobalt with a lower oxidation state to cobalt with a higher oxidation state increased significantly. All of these results indicated that electron cloud density around the Co atoms increased when Fe^{3+} ions were doped. According to the high-resolution Fe 2p XPS spectra of Fe-doped Co_4S_3/Co_9S_8 NS (Fig. S8 in Supporting information), it can be seen that the binding energies of Fe $2p_{3/2}$ and Fe $2p_{1/2}$ were at about 713.2 eV and 725.0 eV, respectively, and exhibited positively shifted [42], further verifying the electron transfer from Fe element to Co. The electron transfer between Fe and Co makes the Lewis acid of Co stronger, which was more conducive to the adsorption of OH^- molecules (Lewis base), making the formation of intermediate products easier and weakening the surface adsorption capacity of toxic intermediates. All of these facts are conducive to the improvement of catalytic

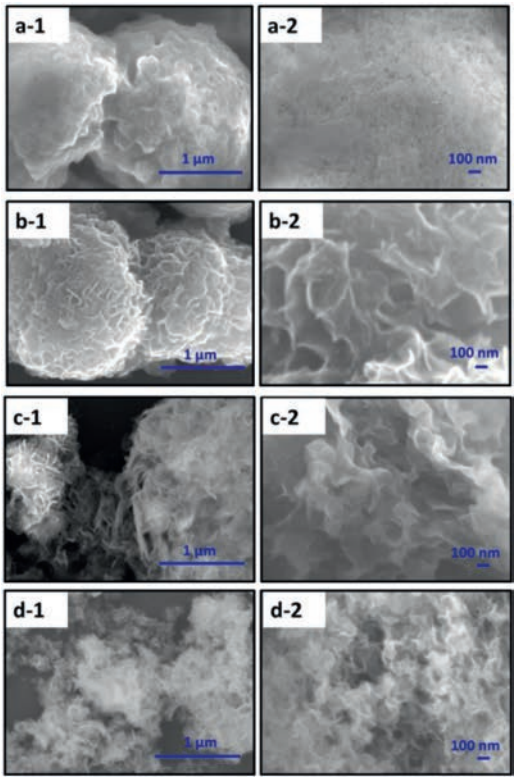

Fig. 8. SEM images of the prepared (a) Fe-doped Co_4S_3/Co_9S_8 NS, (b) Cr-doped Co_4S_3/Co_9S_8 NS, (c) Mn-doped Co_4S_3/Co_9S_8 NS and (d) Ni-doped Co_4S_3/Co_9S_8 NS with different magnification.

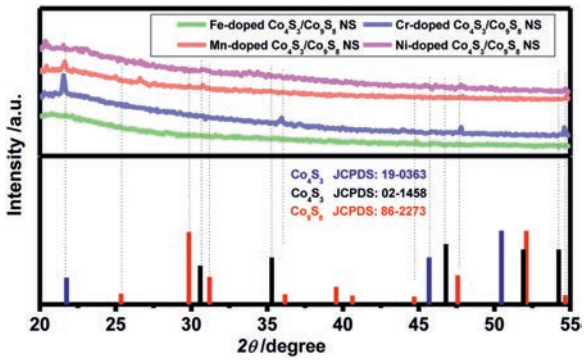

Fig. 10. XRD patterns of the prepared M-doped Co_4S_3/Co_9S_8 NS (M = Fe^{3+}, Cr^{3+}, Mn^{2+} and Ni^{2+}).

activity and stabilityof the catalyst. Similar phenomena and conclusions also apply to the doping of Cr^{3+} or Mn^{2+} ions. The difference was that the doping of these two ions only gave a relatively small negative shift of the Co 2p orbital binding energy. From the Fig. 7a, the typical peaks corresponding to the chemical states of Co^{2+} $2p_{3/2}$ and Co^{3+} $2p_{3/2}$ in Mn-doped Co_4S_3/Co_9S_8 NS exhibited 0.6 eV and 2.0 eV negative shifts with the position of Co $2p_{1/2}$ unchanged. The doping of Mn^{2+} ions displayed 0.4 eV negative shifts only for the binding energy of Co $2p_{3/2}$. The peak assigned to Co^{2+} $2p_{1/2}$ did not exhibit. Therefore, compared with the Fe-doped Co_4S_3/Co_9S_8 NS catalyst, although the doping of Cr^{3+} or Mn^{2+} ions can also regulate the electron cloud around cobalt atoms and make the binding energy of cobalt ions shift negatively, the role to enhance OER performance of Co_4S_3/Co_9S_8 NS was not as good as that of iron ions doping. Conversely, the incorporation of Ni^{2+} led Co $2p_{3/2}$ a remarkable 0.4 eV positive shifts. It was induced that

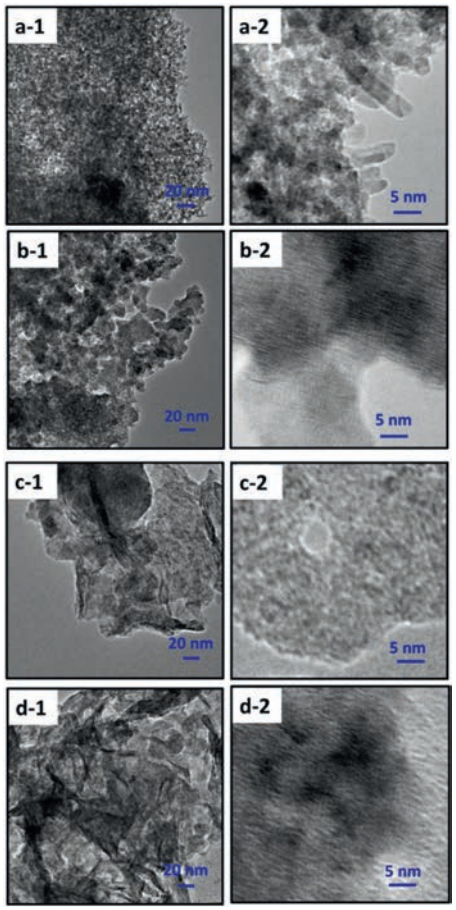

Fig. 9. TEM images of the prepared (a) Fe-doped Co_4S_3/Co_9S_8 NS, (b) Cr-doped Co_4S_3/Co_9S_8 NS, (c) Mn-doped Co_4S_3/Co_9S_8 NS and (d) Ni-doped Co_4S_3/Co_9S_8 NS with different magnification.

electron cloud density aroundthe Co atoms decreased when Ni^{2+} ions were doped. Therefore, an beneficial redistribution of charge at the interface due to an electronic interaction between the doped Ni^{2+} ions and Co_4S_3/Co_9S_8 NS would result in the lower electrocatalytic activity [43]. Different from that the negative shift of Co 2p would enhance the OER catalytic activity and the more negative, the higher the activity, the negative shift of S 2p would lower the OER activity and the more negative, the less active. This is consistent with our experimental results. As exhibited in Fig. 7b, compared with undoped Co_4S_3/Co_9S_8 NS, both the binding energies of S $2p_{3/2}$ and S $2p_{1/2}$ showed a remarkable 1.1 eV and 0.6 eV positive shifts in Fe-doped Co_4S_3/Co_9S_8 NS, the OER activities of which improves obviously. The smaller positive shifts of S $2p_{3/2}$ and S $2p_{1/2}$ in Cr-doped Co_4S_3/Co_9S_8 NS and Mn-doped Co_4S_3/Co_9S_8 NS only demonstrated just a little better than undoped Co_4S_3/Co_9S_8 NS. In contrast, Ni-doped Co_4S_3/Co_9S_8 NS displayed the lower OER catalysis activity than undoped Co_4S_3/Co_9S_8 NS evidenced by the conspicuous negative shifts of S $2p_{3/2}$ and S $2p_{1/2}$.

Figs. 8 and 9 showed the SEM and TEM images of the prepared M-doped Co_4S_3/Co_9S_8 NS (M = Fe^{3+}, Cr^{3+}, Mn^{2+} and Ni^{2+}) with different magnification. Similar to the case of Co_4S_3/Co_9S_8 NS, Ni-doped Co_4S_3/Co_9S_8 NS still maintained the discrete two-dimensional sheet morphology (Figs. 8a and 9a). It is important to note, however, the morphologies of Co_4S_3/Co_9S_8 NS doped with Fe, Cr and Mn ions both have a tendency to assemble into 3D microspheres. That is to say, after the addition of Fe^{3+}, Cr^{3+}, or Mn^{2+} ions, 2D nanosheet was converted into 3D microsphere morphology, thus resulted in the improvement of electrocatalytic activity

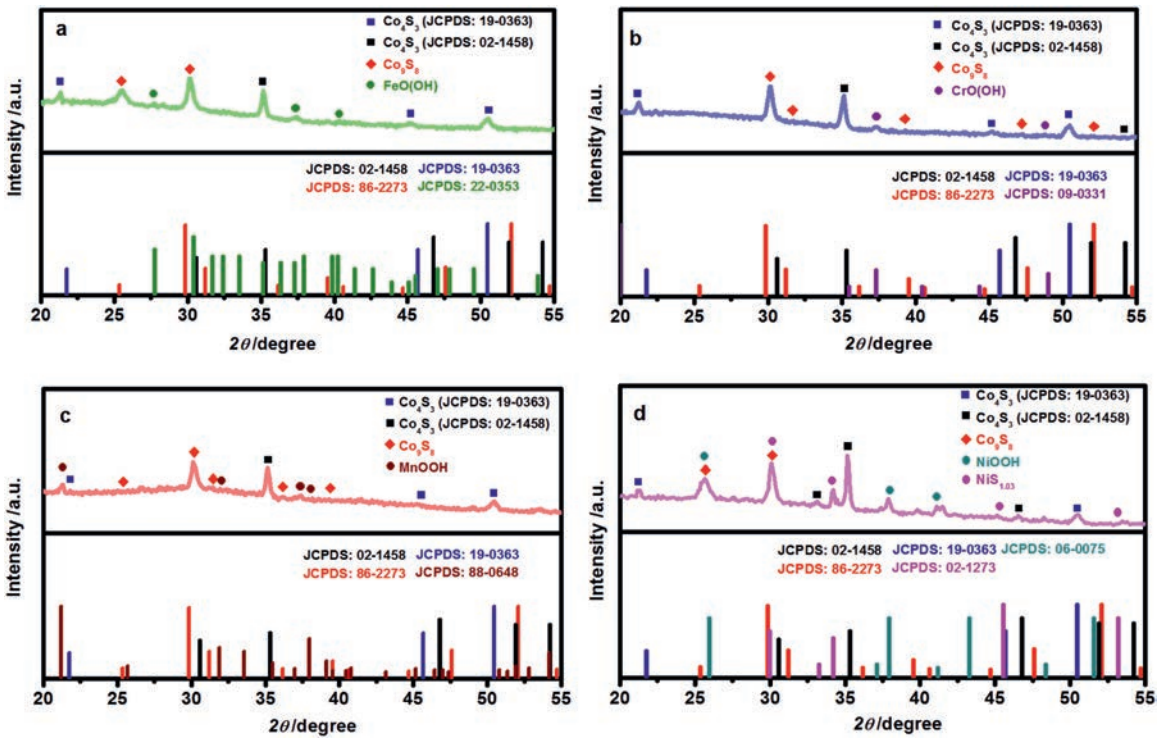

Fig. 11. XRD patterns of the prepared (a) Fe-doped Co_4S_3/Co_9S_8 NS, (b) Cr-doped Co_4S_3/Co_9S_8 NS, (c) Mn-doped Co_4S_3/Co_9S_8 NS and (d) Ni-doped Co_4S_3/Co_9S_8 NS after OER reaction.

toward OER. The trend obeyed the order of Fe-doped Co_4S_3/Co_9S_8 NS > Cr-doped Co_4S_3/Co_9S_8 NS > Mn-doped Co_4S_3/Co_9S_8 NS, consistent with the order of OER performance. The 3D microsphere morphology of Cr-doped Co_4S_3/Co_9S_8 NS and Mn-doped Co_4S_3/Co_9S_8 NS was composed of lamellar structures, respectively. The difference was that the two-dimensional sheet structure of Cr-doped Co_4S_3/Co_9S_8 NS (Figs. 8b and 9b) was smaller than that of Mn-doped Co_4S_3/Co_9S_8 NS (Figs. 8c and 9c). The smaller two-dimensional lamellae of Cr-doped Co_4S_3/Co_9S_8 NS allowed more active sites to be exposed, resulting in slightly higher OER activity compared with Mn-doped Co_4S_3/Co_9S_8 NS. For the typical Fe-doped Co_4S_3/Co_9S_8 NS, which similarly possessed 3D distinctive microsphere structure composed of 1D nanostructure and smallest 2D lamellae (Figs. 8d and 9d), the OER performance was much inferior to Cr-doped Co_4S_3/Co_9S_8 NS and Mn-doped Co_4S_3/Co_9S_8 NS, reflecting in the lowest tafel slope and smallest charge transfer resistance. These results demonstrated that such a special 3D structure formed by Fe^{3+} doping efficiently facilitated electron transfer and then enhanced the OER performance.

The XRD patterns of the prepared M-doped Co_4S_3/Co_9S_8 NS (M = Fe^{3+}, Cr^{3+}, Mn^{2+} and Ni^{2+}) were illustrated in Fig. 10. It was obvious that the crystallinity of the four samples decreased a lot after the doping of the four kinds of metal ions, and it was difficult to confirm the structures and states of the doped ions existed in Co_4S_3/Co_9S_8 NS. In addition, a very interesting phenomenon that the origin structure of Co_4S_3 had also been partially transformed with the introduction of metal ion dopants, emerged similarly to the observed transition of crystalline phase for Co_4S_3/Co_9S_8 NS after OER reaction.

In order to further analyze the reasons for the different effects of four doping ions on the OER reaction properties of Co_4S_3/Co_9S_8 NS, the XRD patterns of the prepared M-doped Co_4S_3/Co_9S_8 NS (M = Fe^{3+}, Cr^{3+}, Mn^{2+} and Ni^{2+}) after OER reaction were also measured and the results were exhibited in Fig. 11, respectively. Apparently, all the doped metal ions existed in 3+ oxidation state, *i.e.*, MOOH (M = Fe, Cr, Mn and Ni) under OER conditions. Among them, FeOOH and CrOOH, the formation of which did not involve the change of valence state, these so-called active substances contributed to the increased OER activity of Co_4S_3/Co_9S_8 NS, as reported in the literatures [44,45]. Even though the valence state of manganese has changed, the resulted Mn^{3+} of MnOOH was great important to achieve high activity of OER according to the Dai' group work [46]. However, the formation of γ-NiOOH resulted from the $Ni(OH)_2$ during the OER process would lead a much more severe distortion of the oxygen octahedra around the Ni ions. Such an irreversibly deactivated Ni redox sites had little OH^- affinity and thus obstructed the OER process [47].

Moreover, just to figure out the stability, we examined the catatlyst after the stability tests. SEM images in Figs. S9b-e (Supporting information) revealed that the morphologies of the prepared Fe-doped Co_4S_3/Co_9S_8 NS, Cr-doped Co_4S_3/Co_9S_8 NS, Mn-doped Co_4S_3/Co_9S_8 NS, and Ni-doped Co_4S_3/Co_9S_8 NS remained largely unchanged after the CP tests. Co_4S_3/ Co_9S_8 NS, however, as exhibited in Fig. S9a (Supporting information), did have a slight change in morphology compared with the fresh Co_4S_3/Co_9S_8 NS. Fig. S10 (Supporting information) compared the XRD patterns of the prepared Co_4S_3/Co_9S_8 NS, Fe-doped Co_4S_3/Co_9S_8 NS, Cr-doped Co_4S_3/Co_9S_8 NS, Mn-doped Co_4S_3/Co_9S_8 NS and Ni-doped Co_4S_3/Co_9S_8 NS after OER reaction and after CP stability tests. From the XRD patterns of Fe-doped Co_4S_3/Co_9S_8 NS, Cr-doped Co_4S_3/Co_9S_8 NS, and Mn-doped Co_4S_3/Co_9S_8 NS, it was observed that the two diffraction peaks attributed to the (100) and (101) planes of Co_4S_3 disappeared for the three samples, while the diffraction peaks attributed to the (220) crystal plane of Co_9S_8, which existed in Fe-doped Co_4S_3/Co_9S_8 NS and non-existed in Cr-doped Co_4S_3/Co_9S_8 NS and Mn-doped Co_4S_3/Co_9S_8 NS before CP test, were enhanced in Fe-doped Co_4S_3/Co_9S_8 NS and appeared in the latter two samples after the stability test. But for the XRD patterns of Co_4S_3/Co_9S_8 NS and Ni-doped Co_4S_3/Co_9S_8 NS, the two diffraction peaks attributed to the (100) and (101) planes of Co_4S_3

still remained the same. The difference was that, the (220) crystal plane of Co_9S_8, which existed in Co_4S_3/Co_9S_8 NS and Ni-doped Co_4S_3/Co_9S_8 NS before CP tests, both vanished. At the same time, the other diffraction peak attributed to the (331) crystal plane of Co_9S_8 also disappeared in Ni-doped Co_4S_3/Co_9S_8 NS after the stability test. Thus, combined with the different effects on the OER catalytic activity and stability of Co_4S_3/Co_9S_8 NS resulted by different metal ion doping, all the features discussed above indicated that the existence of Co_9S_8 phase may have a positive effect on the enhanced stability, and conversely that the Co_4S_3 phase may have a negative influence, which may be due to the higher stability of Co_9S_8 than Co_4S_3.

In summary, Co_4S_3/Co_9S_8 nanosheets (Co_4S_3/Co_9S_8 NS) were successfully synthesized *via* an efficient solvothermal process combined with ultrasonic exfoliation in this paper. The dopant of different metal ions (M = Fe^{3+}, Cr^{3+}, Mn^{2+} and Ni^{2+}) into Co_4S_3/Co_9S_8 NS by a simple cation exchange method exhibited different effects on the OER electrocatalytic properties of Co_4S_3/Co_9S_8 NS. Among them, Fe-doped Co_4S_3/Co_9S_8 NS showed the fairly better OER catalytic activity compared with undoped Co_4S_3/Co_9S_8 NS. The OER catalysis activities of Cr or Mn-doped Co_4S_3/Co_9S_8 NS were just a little better than undoped Co_4S_3/Co_9S_8 nanosheets. Conversely, Co_4S_3/Co_9S_8 NS exhibited weakened OER activity after the Ni^{2+} ions doping. Evidenced by XPS spectra, the reasons for enhancing or weakening OER activities of the Co_4S_3/Co_9S_8 NS resulted from the redistribution of charge at the interface due to an electronic interaction between the doped metal ions and Co_4S_3/Co_9S_8 NS.

Declaration of competing interest

The authors declare that they have no known competing financial interests or personal relationships that could have appeared to influence the work reported in this paper.

Acknowledgments

This work was supported by the National Natural Science Foundation of China (Nos. 21671179, 21705117, 21904120 and 62073299), Henan Province Science and Technology Programs (Nos. 202102210045 and 212102310858), and Program for Innovative Research Team (in Science and Technology) in University of Henan Province (No. 20IRTSTHN017).

Supplementary materials

Supplementary material associated with this article can be found, in the online version, at doi:10.1016/j.cclet.2021.08.019.

References

[1] Z.W. Seh, J. Kibsgaard, C.F. Dickens, et al., Science 355 (2017) eaad4998.
[2] X.Y. Chia, M. Pumera, Nat. Catal. 1 (2018) 909–921.
[3] C.L. Bentley, M. Kang, P.R. Unwin, J. Am. Chem. Soc. 141 (2019) 2179–2193.
[4] L.L. Cao, Q.Q. Luo, J.J. Chen, et al., Nat. Commun. 10 (2019) 4849.
[5] K.S. Exner, H. Over, ACS Catal. 9 (2019) 6755–6765.
[6] J.H. Wang, W. Cui, Q. Liu, et al., Adv. Mater. 28 (2016) 215–230.
[7] Y.L. Liu, X.H. Luo, C.L. Zhou, et al., Appl. Catal. B: Environ. 260 (2020) 118197.
[8] D.H. He, X.L. Wu, W. Liu, et al., Chin. Chem. Lett. 30 (2019) 229–233.
[9] Z.L. Chen, R.B. Wu, M. Liu, et al., J. Mater. Chem. A 6 (2018) 10304–10312.
[10] S.L. Zhang, D. Zhai, T.T. Sun, et al., Appl. Catal. B: Environ. 254 (2019) 186–193.
[11] Y.R. Li, Q.F. Guo, Y.M. Jiang, et al., Chin. Chem. Lett. 32 (2021) 755–760.
[12] S.F. Fu, C.Z. Zhu, J.H. Song, et al., ACS Appl. Mater. Inter. 9 (2017) 36755–36761.
[13] N. Zhang, Y. Wang, Y.C. Hao, et al., Nanoscale 10 (2018) 20313–20320.
[14] Q. Zhao, Z.H. Yan, C.C. Chen, et al., Chem. Rev. 117 (2017) 10121–10211.
[15] M.K. Bates, Q.Y. Jia, H. Doan, et al., ACS Catal. 6 (2016) 155–161.
[16] X.T. Han, C. Yu, S. Zhou, et al., Adv. Energy Mater. 7 (2017) 1602148.
[17] B. Cao, C.H. Luo, J. Lao, et al., ACS Omega 4 (2019) 16612–16618.
[18] C. Mahala, M. Devi Sharma, M. Basu, ChemElectroChem 6 (2019) 3488–3498.
[19] P. Shi, X.D. Cheng, S.L. Lyu, Chin. Chem. Lett. 32 (2021) 1210–1214.
[20] F. Rodríguez-Hernández, D.C. Tranca, A. Martínez-Mesa, et al., J. Phys. Chem. C 120 (2016) 25851–25860.
[21] C.P. Hao, H. Lv, Q. Zhao, et al., Int. J. Hydrogen Energ. 42 (2017) 9384–9395.
[22] Y. Yang, L.C. Kao, Y.Y. Liu, et al., ACS Catal. 8 (2018) 4278–4287.
[23] Y.F. Zhao, J.Q. Zhang, W.J. Wu, et al., Nano Energy 54 (2018) 129–137.
[24] W.K. Gao, J.F. Qin, K. Wang, et al., Appl. Surf. Sci. 454 (2018) 46–53.
[25] Z.Q. Xie, H. Tang, Y. Wang, ChemElectroChem 6 (2019) 1206–1212.
[26] Y.W. Liu, C. Xiao, M.J. Lyu, et al., Angew. Chem. Int. Ed. 54 (2015) 11231–11235.
[27] Y.W. Liu, H. Cheng, M.J. Lyu, et al., J. Am. Chem. Soc. 136 (2014) 15670–15675.
[28] M.R. Gao, W.T. Yao, H.B. Yao, et al., J. Am. Chem. Soc. 131 (2009) 7486–7487.
[29] L.L. Feng, G.D. Li, Y.P. Liu, et al., ACS Appl. Mater. Inter. 7 (2015) 980–988.
[30] L. Yin, L.Q. Wang, X.H. Liu, et al., Eur. J. Inorg. Chem. 14 (2015) 2457–2462.
[31] S.J. Peng, X.P. Han, L.L. Li, et al., Small 12 (2016) 1359–1368.
[32] L.L. Feng, M.H. Fan, Y.Y. Wu, et al., J. Mater. Chem. A 4 (2016) 6860–6867.
[33] X.T. Feng, Q.Z. Jiao, T. Liu, et al., ACS Sustain. Chem. Eng. 6 (2018) 1863–1871.
[34] B.K. Barman, K.K. Nanda, Dalton Trans. 45 (2016) 6352–6356.
[35] A.G. Butterfield, C.R. McCormick, J.M. Veglak, et al., J. Am. Chem. Soc. 43 (2021) 7915–7919.
[36] D.H. Son, S.M. Hughes, Y.D. Yin, et al., Science 306 (2004) 1009–1012.
[37] B.J. Beberwyck, Y. Surendranath, A.P. Alivisatos, J. Phys. Chem. C 117 (2013) 19759–19770.
[38] L. De Trizio, L. Manna, Chem. Rev. 116 (2016) 10852–10887.
[39] F. Song, X.L. Hu, J. Am. Chem. Soc. 136 (2014) 16481–16484.
[40] B. Wang, Y.Z. Ye, L. Xu, et al., Adv. Func. Mater. 30 (2020) 2005834.
[41] F.L. Gong, S. Ye, M.M. Liu, Nano Energy 78 (2020) 105284.
[42] J. Jiang, S. Lu, H. Gao, et al., Nano Energy 27 (2016) 526–534.
[43] J.F. Qin, M. Yang, S. Hou, et al., Appl. Surf. Sci. 502 (2020) 144172.
[44] M. Yang, J.Y. Xie, W.L. Yu, et al., ACS Appl. Mater. Interfaces 13 (2021) 17450–17458.
[45] Y. Yang, L.N. Dang, M.L. Shearer, et al., Adv. Energy Mater. 8 (2018) 1703189.
[46] M.L. Cui, H.H. Zhao, X.P. Dai, et al., ACS Sustainable Chem. Eng. 7 (2019) 13015–13022.
[47] A. Mavric, M. Fanetti, Y.T. Lin, et al., ACS Catal. 10 (2020) 9451–9457.